Nanotechnology Perceptions
ISSN 1660-6795
www.nano-ntp.com

An Integrated Hybrid Approach for Efficient Brain Tumor Analysis Using Magnetic Resonance Imaging: Preprocessing, Feature Extraction, Optimization, and Classification

Pavan Kumar Pagadala[1,2], Malathy Batumalay[2], Sudha Narang[3], Trinath Basu Miriyala[1], Chidambaranathan C M[4], Basi Reddy A[5]

[1]Department of Computer Science and Engineering, Koneru Lakshmaiah Education Foundation, Aziz Nagar, Hyderabad, Telangana-500075, India.
[2]Faculty of Data Science and Information Technology, INTI International University, 71800 Nilai, Negeri Sembilan, Malaysia.
[3]Maharaja Agrasen Institute of Technology, Sector 22, Rohini, Delhi.
[4]Department of Computer Science and Engineering, School of Computing, Vel Tech Rangarajan Dr.Sagunthala R&D Institute of Science and Technology, Chennai, India.
[5]Department of Computer Science and Engineering, School of Computing, Mohan Babu University, Tirupati, Andhra Pradesh, India

The diagnosis of brain tumours in a timely and accurate manner is critical for effective therapy. Using MRI data, we offer an integrated hybrid approach for efficient brain tumor analysis. The technique is divided into five steps that handle various aspects of the analysis process. MRI scans are preprocessed in the first stage using scaling and filtering techniques to standardize and improve picture attributes. The second stage focuses on feature extraction by employing the Gray-Level Co-occurrence Matrix (GLCM) method to distinguish tumour and non-tumour regions. Particle Swarm Optimization (PSO) is used in the third stage to optimize specific features. In the fourth stage, a Convolutional Neural Network (CNN) and Support Vector Machine (SVM) combination is employed for tumour detection and classification, allowing for precise tumour location. The suggested hybrid strategy is evaluated for performance in the final stage, reaching high metrics such as specificity (99.573%), accuracy (99.8681%), precision (99.439%), recall (98.45%), and F1 score (99.225%). The goal of this research is to create an accurate and efficient method for brain tumour analysis, answering the demand for better diagnosis. To provide a reliable and exact study of brain tumours, the integrated hybrid methodology combines preprocessing, feature extraction, optimization, detection, and classification.

Keywords: Feature extraction, Gray-Level Co-occurrence Matrix (GLCM), Particle Swarm Optimisation (PSO), Convolutional Neural Network (CNN), Support Vector Machine (SVM), Tumour detection, Classification.

1. Introduction

The importance of digital information in the diagnosis of diseases, particularly brain tumours, cannot be emphasised in today's digital world [1]. Medical images obtained using techniques such as Magnetic Resonance Imaging (MRI) give critical data for the accurate and efficient identification of disorders [2]. These digital materials are easily kept, shared, and analysed, allowing healthcare providers to make informed patient care decisions. Computer vision is critical in utilising these digital assets for illness detection [3-5]. Medical experts can extract useful information from medical photos by using computer vision algorithms and techniques [6]. Computer vision algorithms are meant to analyse and interpret visual data automatically, allowing for the detection of patterns, structures, and abnormalities in medical images. This improves the accuracy and efficiency of illness detection, localisation, and classification, including brain tumours [7-9]. The brain's importance in the human body cannot be emphasised [10]. The brain is the central nervous system's command centre, coordinating different physical functions and cognitive processes [11-14]. Any anomaly or disease affecting the brain, such as tumour growth, can have serious consequences for an individual's health and well-being [15]. Brain tumours, in particular, can affect normal brain function, resulting in neurological symptoms, cognitive deficits, and possibly fatal illnesses [16-18]. Tumours in the brain can put pressure on surrounding tissues, resulting in a variety of symptoms depending on their location, size, and kind. Common symptoms include recurrent headaches, seizures, visual problems, motor skill impairments, cognitive decline, and personality changes [19].

Brain tumours are a major public health concern, and early identification is important for effective treatment and better patient outcomes [20]. If not detected early, these aberrant brain growths can cause severe neurological consequences and even death. As a result, there is an urgent need for reliable and effective techniques of detecting brain tumours at the appropriate time [21-23]. Advances in computer vision, machine learning, and deep learning have showed considerable promise in medical image analysis in recent years, providing valuable tools for brain tumour detection and classification. [24] These methods make use of the power of algorithms and models to analyse complicated patterns and features in medical imaging data, resulting in more accurate and trustworthy diagnoses. The intention to contribute to the development of better tools for brain tumour analysis drives this research. The major goal is to improve the diagnostic process and enable early detection of brain tumours so that timely intervention and personalised treatment methods may be implemented. Here the best methodology for the precise brain tumour detection by using the intrinsic information and structures available in MRI scans using computer vision and advanced learning AI methods is to be developed [25].

Despite advances in medical imaging and processing tools, existing methods for detecting brain tumours continue to encounter obstacles [26]. These include the necessity for human knowledge in analysing complex medical images, as well as limited accuracy and inefficiency. These constraints can cause a delay in diagnosis and consequently jeopardise patient outcomes [27]. As a result, the challenge is to create a superior methodology that overcomes these limitations while still offering accurate and rapid brain tumour analysis from MRI data.

The following research questions will lead our analysis in order to address the problem statement:

- How might computer vision with latest methods be used to progress brain tumour identification and classification from MRI scans?
- What are the main obstacles and limits of the current approaches for analyzing brain tumours using these techniques?
- How can the proposed integrated approach, which combines stages of pre-processing, feature extraction, optimization, detection and classification, and performance evaluation, address these challenges and achieve superior performance in terms of various parameters?
- How does the suggested method's performance compare to other methodologies for brain tumour analysis published in the literature?

The paper is divided into five major sections to provide an organised summary of the research. Section 1 serves as an introduction, presenting a brief history of brain tumours and emphasising the necessity of early detection. The problem statement is well stated, emphasising the importance of developing an effective method for detecting brain tumours at an early stage. Section 2 provides a detailed review of publications released in the last seven years that cover numerous techniques and approaches utilised in brain tumour analysis. A table comparing and analysing the existing literature is supplied to highlight research gaps. Section 3 delves into the methodology of the suggested Integrated Hybrid approach, outlining the steps and algorithms used in the research. Each level is discussed step by step, and the mathematical formulas for each algorithm are provided. Section 4 describes the experimental studies that were conducted to test the suggested approach. It offers a complete description of the extracted features as well as a comprehensive performance evaluation, reporting measures like as accuracy, precision, recall, and F1 score. Section 5 gives a succinct conclusion summarising the research findings and emphasising their significance. The future scope is examined in order to offer prospective directions for future research. The article finishes with a References section that summarises the sources cited throughout the publication. This organisation ensures a clear and logical presentation of the research, allowing readers to quickly understand the context, methods, experimental results, and overall implications of the study.

2. Literature Review

In 2022, Kesav et al. suggested a RCNN method which was investigated on Kaggle datset [28]and attained an accuracy of 98.21%. The system's key disadvantage is that it is confined to object detection. Furthermore, the training and inference processes for RCNN models usually need advanced technology and extensive processing periods, rendering them unsuitable for real-time or resource-constrained applications. Furthermore, the RCNN technique may fail to detect small or subtle tumour regions since the region proposal stage may miss these areas or generate false positives. While RCNN has demonstrated promise in a variety of computer vision tasks, its limitations in terms of processing complexity and detection accuracy for brain tumour investigation should be considered before employing this technology.

In 2021, Özlem et al. suggested to utilize transfer learning method [29] and attained an overall accuracy of 99.02%. Limited availability of labeled data specific to brain tumours can restrict

the effectiveness of transfer learning approaches. Moreover, the generalizability of the pre-trained model may be affected by the differences between the source task and the target task, leading to suboptimal performance. While transfer learning can accelerate the development of models for brain tumour detection, the reliance on high-quality and representative datasets remains a significant limitation. Efforts to acquire larger and more diverse datasets specific to brain tumours are necessary to fully exploit the potential of transfer learning in this domain.

In 2021, Srikanth et al. presented [30] a 16-layer VGG-16 deep NN as their proposed model. The authors attained an outcome, which have a 98 percent accuracy. The VGG-16 architecture has demonstrated promising results in a variety of computer vision tasks, including image classification, because to its depth and large number of trainable parameters. However, when it comes to detecting brain tumours, the limited quantity and variety of available datasets can be a problem. Because of the complexity of brain tumour imaging data, as well as the probable scarcity of labelled samples, the model may memorise the training data rather than generalising successfully to unknown cases. When applied to new and different brain tumour images, this overfitting issue can result in decreased performance and a lack of robustness.

In 2020, GS Tandel et al. [31] suggested a transfer learning-based type of a CNN and it achieved a mean accuracy of 98.5 %. Transfer learning necessitates the use of a formerly learned CNN model that has been trained on a big and diverse dataset. Finding a pre-trained model specifically tailored for brain tumour detection, on the other hand, can be difficult. This may result in the use of models trained on more broad image datasets, which may not correctly capture the particular traits and characteristics of brain tumours.

In 2019, Deepak et al. [32] suggested to use CNN model with a pre-trained GoogleNet. The reliance on pre-trained models limits the network architecture's ability to be fine-tuned and adapted specifically for brain tumour detection. Different datasets and imaging modalities may necessitate customised network setups to successfully capture the essential information. The model's inability to be fine-tuned substantially may limit its ability to detect and categorise brain tumours effectively and a property of overfitting was also noticed in this method. However, it attained an accuracy of 98%.

In 2019, Gumaei et al. [33] suggested to use Principal Component Analysis (PCA) with Regularized Extreme Learning Machine (RELM) classification. PCA presupposes that the data is normally distributed and follows a linear relationship. If these assumptions are broken, PCA performance may suffer. Nonlinear interactions and non-normal distributions can lead to distorted or biassed main components, which can lead to incorrect dimensionality reduction and feature extraction. The results reported 94.23% accuracy.

In 2018, Abiwinanda et al suggested a CNN along with ‘adam’ optimizer [34] and produced an accuracy of 98.51%. CNNs with the “adam” optimizer necessitate meticulous adjustment of hyperparameters. The Adam optimizer's learning rate, beta1, beta2, and epsilon settings can all have a major impact on the training process and convergence. The following Table 1 presents an engaging comparative discussion of the above topics.

Table 1. Comparative discussion of previous methods

S.No.	Technique Used	Year of Publication	Observations	Parameters Attained	Gaps/Limitations
1.	RCNN approach [28]	2022	Used Public database Kaggle for carrying out the entire work	Accuracy: 98.21 %	The biggest disadvantage is that it is only capable of detecting objects.
2.	Transfer learning [29]	2021	Uses pre-trained model with vast amount of data	Accuracy: 99.02%	generalizability of the pre-trained model
3.	a 16-layer VGG-16 deep NN [30]	2021	Images are subjected to be improved for their resolution	Accuracy: 98%	the limited quantity and variety of available datasets can be a problem
4.	TL based CNN [31]	2020	Authors used standard and basic ML algorithms also.	Accuracy: 94.70%, Recall :98.70%, Precision: 98.60 %, F-score: 99.98%	Transfer learning necessitates the use of a previously learned CNN model
5.	CNN technique + GoogleNet [32]	2019	Pre-trained model is utilized here.	Accuracy: 98%, Recall :97.9%, Precision: 99.2 %, Specificity: 99.4%, F-score: 97%	phenomenon of overfitting with smaller training data
6.	PCA+RELM [33]	2019	Feature extraction with Principal Component Analysis	Accuracy: 94.23%	PCA presupposes that the data is normally distributed and follows a linear relationship
7.	CNN+adam Optimizer [34]	2018	A principle of Stochastic form of Gradients are utilized	Accuracy: 98.51%	Suboptimal hyperparameter selection can result in sluggish convergence
8.	Conventional CNN [35]	2018	Features were extracted using the simple CNN	accuracy of 93.68%, Recall :97.5%, Precision: 91 %, F-score: 94.1%	non-linear character of Conventional CNN features
9.	Deep Learning [36]	2017	2 types of neural networks are utilized	accuracy of 91.43%, Recall :98%, Precision: 93 %, F-score : 95%	exact reasoning behind the decision-making process is frequently unclear

Suboptimal hyper parameter selection can result in sluggish convergence, unstable training, or even failure to converge. Finding the appropriate selection of hyper parameters for a specific problem can be difficult, and lengthy testing and fine-tuning may be required.

In 2018, Pashaei et al. [35] presented a simple and traditional CNN procedure along with its model and 93.68%. of accuracy was determined here. While CNNs excel at feature extraction, comprehending the learnt representations can be difficult. The high-dimensional and non-linear character of Conventional CNN features makes understanding the underlying significance of certain features or the network's decision-making process difficult.

In 2017, Paul et al. [36] used deep learning methods to attain 91.43%.of accuracy where basic Deep Learning models create predictions based on data patterns learnt, but the exact reasoning behind the decision-making process is frequently unclear. This lack of transparency can be

problematic in areas where accountability and transparency are critical, such as healthcare and judicial systems.

The review of the literature reveals significant shortcomings in current methodologies for brain tumour analysis. Although effective for object recognition, the RCNN technique lacks the fine segmentation needed for correct diagnosis and is computationally demanding, rendering it unsuitable for real-time or resource-constrained applications. Transfer learning approaches rely on limited labelled data from brain tumours and may not generalise effectively to other tasks, demanding larger and more diversified datasets.

The review of the literature reveals significant shortcomings in current methodologies for brain tumour analysis. Although effective for object recognition, the RCNN technique lacks the fine segmentation needed for correct diagnosis and is computationally demanding, rendering it unsuitable for real-time or resource-constrained applications. Transfer learning approaches rely on limited labelled data from brain tumours and may not generalise effectively to other tasks, demanding larger and more diversified datasets. While accurate in other tasks, the VGG-16 deep neural network suffers with limited and heterogeneous brain tumour datasets, resulting in overfitting and poor robustness. CNN approaches' reliance on pre-trained models restricts adaptability and may necessitate customised setups for diverse datasets. The assumption of linear correlations and normal distribution in Principal Component Analysis (PCA) has an impact on accurate feature extraction. The "adam" optimizer is difficult to use for CNN hyperparameter adjustment, and understanding the learnt representations and decision-making process of CNNs can be difficult due to its high-dimensional and non-linear nature. These constraints emphasise the importance of better segmentation, larger datasets, customised models, a better understanding of learning features, and transparent decision-making procedures in brain tumour analysis.

To address these shortcomings, the proposed method provides an integrated hybrid strategy for efficient brain tumour analysis. This method tries to overcome the limitations of prior methods by offering more exact tumour localization and employing a hybrid strategy that integrates several methodologies for increased accuracy.

3. Methodology and Algorithm

The diagram provided in Fig. 1 depicts the proposed procedure for diagnosing brain tumours, which includes five distinct stages. The input MRI scans are resized, the Median filter is applied, and the Haar wavelet decomposition is performed during the pre-processing stage. These techniques aid in image standardisation and enhancement of vital characteristics while decreasing noise. The feature extraction in the upcoming stage is done using GLCM method. Textural information is captured by GLCM, allowing for better distinction of tumour and non-tumour regions. The final stage entails optimising the selected characteristics using Particle Swarm Optimisation (PSO). PSO traverses the feature space effectively, maximising discriminative power. The fourth stage employs a CNN and SVM to combine detection and classification. By segmenting the brain tumour area, this combination allows for exact tumour localization. Finally, the performance evaluation stage quantifies the effectiveness of the suggested strategy. This image depicts the workflow of the projected technique and illustrates

its probable for higher performance in brain tumour diagnostics.

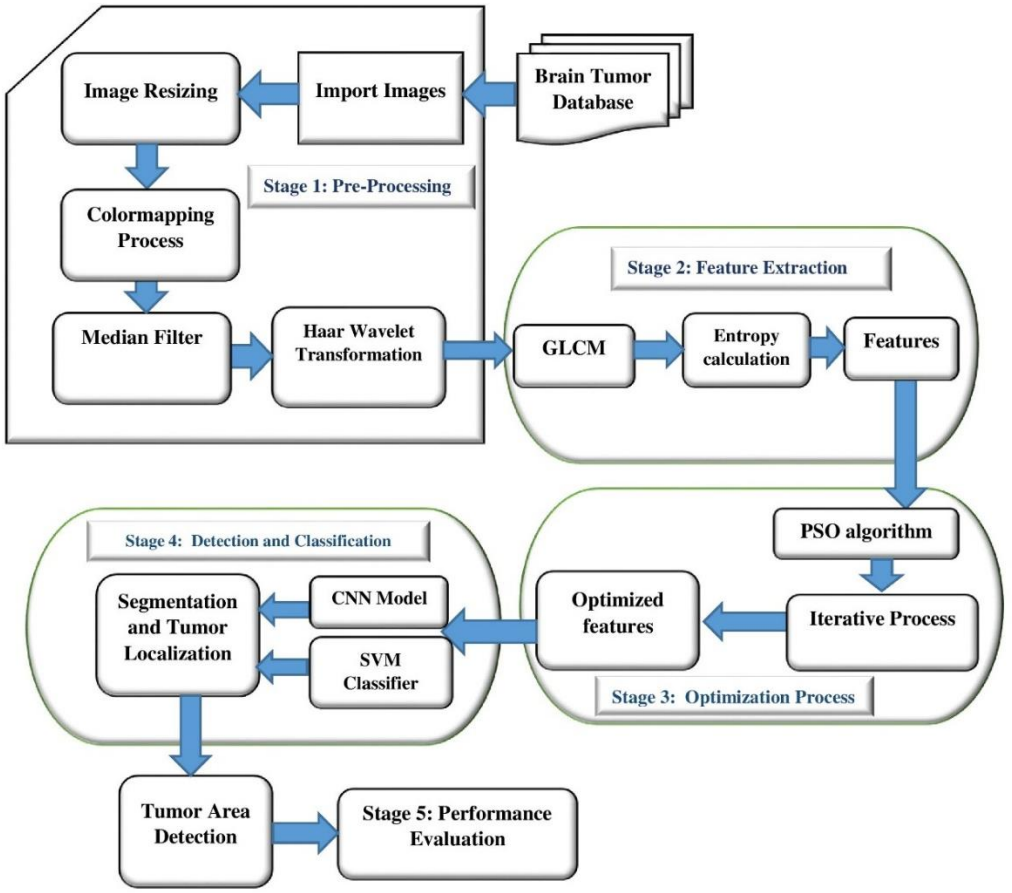

Fig. 1. Block Diagram of Proposed Algorithm

A. Algorithm for Stage 1 : Pre-Processing

Step i. Set the path or directory to the location where the brain tumour MR scan images are stored.

Step ii. Read and import the images from the specified directory of MR Brain Scan Image Dataset which is acquired from Kaggle [37] which contains 300 samples of Brain MR Scans.

Step iii. Set the desired dimensions for the resized image (e.g., width and height)

Step iv. Iterate through each imported image and Resize each image to the specified dimensions using bilinear interpolation.

Step v. Check if the imported Brain Scan image is available in RGB format, convert it to grayscale by eliminating the hue and saturation information while retaining the luminance.

Step vi. Apply a median filter to the image to remove artifacts and improve image quality.

a. Given:

Input image: I(x, y), say (x, y) denotes the pixel coordinates.

Window size: N x N, where N is an odd integer.

b. Initialize an empty output image, O(x, y), with the same dimensions as the input image.

c. Determine the window region centered around (x, y) with size N x N. b. Initialize an empty list, pixel_values.

d. For each pixel (i, j) within the window region: a. Add the pixel value I(i, j) to the pixel values list and Sort the pixel values list in ascending order.

e. Compute the median value (M) of the sorted pixel values list using the following formula:

$$M = \text{pixel values}\left[\frac{(N \times N + 1)}{2}\right] \quad \ldots\ldots(1)$$

The pixel value at the centre of the N x N block can be calculated using this formula. Within the block, this centre pixel is frequently used as a reference or anchor point to perform different image processing or analysis operations.

f. Set the pixel value attained of the output image at (x, y) to the computed median value (M).

g. Repeat steps b-f for all pixels in the image.

h. Return the output image, O(x, y).

Step vii. Apply Haar wavelet transformation to the image for further analysis by decomposing them into a set of wavelet coefficients

a. Given:

Input image: O(x, y).

Image dimensions: M x N.

b. Initialize an empty set of wavelet coefficients, C.

c. Set the initial approximation image, A_0, as the input image

$$A_0(x, y) = O(x, y) \quad \ldots\ldots(2)$$

The pixel value at coordinates (x, y) in the initial approximation image A0 is denoted by the notation $A_0(x, y)$. In image processing, this notation is commonly used to represent pixel values in a specific image. O(x, y) represents the pixel value at coordinates (x, y) in the input image O on the right side of the equation. We initialize A_0 with the same pixel values as the input image by assigning this value to the corresponding pixel in the initial approximation image A0.

d. Set the level of decomposition, L.

e. For each decomposition level l from 1 to L:

i. Calculate the dimensions of the approximation and detail images at level

ii. Approximation image: $A_l(x, y)$ has dimensions M_l x N_l, where

$$M_l = \text{floor}\left(\frac{M}{2^{l-1}}\right) \quad \text{.....(3)}$$

$$N_l = \text{floor}\left(\frac{N}{2^{l-1}}\right) \quad \text{.....(4)}$$

By systematically applying equations (3) and (4) with increasing "l" values, a series of approximation images with reduced dimensions compared to the previous level can be generated. This hierarchical image representation enables multi-resolution analysis or compression techniques, with higher levels corresponding to lower spatial resolution representations of the original image.

f. Compute the approximation and detail images at level l using the Haar wavelet transformation:

i. Compute the approximation and detail coefficients for the row

Approximation coefficients

$$A_l + 1(r, k) = \frac{(R_{even} + R_{odd})}{\text{sqrt}(2)} \quad \text{.....(5)}$$

Detail coefficients

$$D_l(r, k) = \frac{(R_{even} - R_{odd})}{\text{sqrt}(2)} \quad \text{.....(6)}$$

The approximation coefficients as provided by equation (5) represent the data's coarsest level of approximation. The detail coefficients as provided by equation (6) capture the data's high-frequency components or details. At each level, they represent the differences between the original data and the approximation.

Where

$$R_{even} = A_l(r, 2k) \quad \text{.....(7)}$$

$$R_{odd} = A_l(r, 2k + 1) \quad \text{..... .(8)}$$

ii. Compute the approximation and detail coefficients for the column

Approximation coefficients

$$A_l + 1(k, c) = \frac{(C_{even} + C_{odd})}{\text{sqrt}(2)} \quad \text{.....(9)}$$

Detail coefficients

$$H_l(k, c) = \frac{(C_{even} - C_{odd})}{\text{sqrt}(2)} \quad \text{.....(10)}$$

One can determine the approximation and detail coefficients for the given column of data using the Haar wavelet transformation at each level by sequentially applying these equations. By calculating the approximation and detail coefficients at various levels, we can analyse the data

column at various resolution scales.

Where

$C_{even} = A_l(2k, c)$ ……..(11)

$C_{odd} = A_l(2k + 1, c)$ ……(12)

iii. Store the computed approximation and detail coefficients in the set of wavelet coefficients

$C = \{A_l, H_l, D_l\}$ ……(13)

These coefficients give a thorough representation of the data at various approximation and detail levels, enabling additional processing, analysis, or reconstruction of the initial column of data.

Algorithm for Stage 2: Feature Extraction

Step i. Apply GLCM technique to the filtered image.

a. Given:

Filtered image: F(x, y).

Set of wavelet coefficients as said in equation (13)

b. Initialize an empty GLCM matrix for each component of the filtered image and wavelet coefficients: GLCM_F, GLCM_A_l, GLCM_H_l, GLCM_D_l.

c. Set the desired distance and direction for computing the co-occurrence matrix

d. For each and every point of pixel (x, y) in the filtered image F:

i. Compute the pixel intensity values at the current position and the corresponding pixel at the specified distance and direction

Current pixel intensity

$F_{value} = F(x, y)$ ……..(14)

Co-occurring pixel intensity

$Cooc_{value} = F\big(x + d\cos(\theta), y + d\sin(\theta)\big)$ …….(15)

Where d : distance, θ : direction

The co-occurring pixel intensity in equation (15) represents the intensity value at a specific distance and direction from the current pixel, whereas the current pixel intensity in equation (14) represents the intensity value at a specific position. We can analyse the relationships and characteristics of pixel intensities in an image by evaluating these equations with suitable values, which is helpful for a variety of image processing tasks like feature extraction, texture analysis, and edge detection.

ii. Increment the corresponding entry in the GLCM_F matrix for the current distance and direction:

$$\mathrm{GLCM_F}\,(\mathrm{F_{value}}, \mathrm{Cooc_{value}}) += 1 \quad \ldots\ldots\ldots\ldots\ldots\ldots\ldots\ldots\ldots\ldots\ldots\ldots\ldots\ldots(16)$$

The co-occurrence count or frequency of those intensities is effectively updated by increasing the GLCM_F matrix based on Equation (16) for the current distance, direction, and the corresponding pixel intensities. In order to capture the spatial relationships between pixel intensities in an image, this GLCM matrix is frequently used in texture analysis and pattern recognition tasks.

e. using the wavelet coefficient component instead of the filtered image F, and update the corresponding GLCM matrix

f. Normalize each GLCM matrix by dividing all entries for the corresponding distance and direction, for each GLCM matrix

$$\mathrm{GLCM_{normalized}} = \frac{\mathrm{GLCM}}{\mathrm{sum(GLCM)}} \quad \ldots\ldots\ldots\ldots\ldots\ldots\ldots\ldots\ldots\ldots\ldots\ldots\ldots\ldots(17)$$

Equation (17) explains how to divide each entry of a GLCM (Gray-Level Co-occurrence Matrix) by the total number of entries in the GLCM for the corresponding distance and direction to normalize it.

Step ii. Using the GLCM matrix, calculate the entropy as a measure of the amount of information or randomness in the image.

i. Given:

a. GLCM matrix: $\mathrm{GLCM_{normalized}}$.

b. Initialize the entropy value, entropy = 0

c. Iterate over each entry (i, j) in the $\mathrm{GLCM_{normalized}}$ matrix

d. Compute the probability of occurrence for the current intensity pair

$$\mathrm{P(i,j)} = \mathrm{GLCM\_normalized(i,j)} \quad \ldots\ldots\ldots\ldots\ldots\ldots\ldots\ldots\ldots\ldots\ldots\ldots\ldots\ldots..(18)$$

The probability of occurrence for the current intensity pair (i, j) is determined by equation (18). It shows how likely it is that the intensity pair (i, j) will appear in the image. A higher frequency of occurrence is indicated by higher values.

e. If P(i, j) is non-zero, calculate the entropy contribution E_C for the intensity pair

$$\mathrm{E_C} = -\mathrm{P(i,j)} * \log 2(\mathrm{P(i,j)}) \ldots\ldots\ldots\ldots\ldots\ldots\ldots\ldots\ldots\ldots\ldots\ldots\ldots\ldots\ldots\ldots(19)$$

f. Add the entropy contribution to the overall entropy value

$$\mathrm{entropy} += \mathrm{E_C} \ldots\ldots\ldots\ldots\ldots\ldots\ldots\ldots\ldots\ldots\ldots\ldots\ldots\ldots\ldots\ldots\ldots\ldots\ldots\ldots\ldots\ldots(20)$$

If P(i, j) is greater than zero, equation (19) calculates the entropy contribution for the intensity pair (i, j). Entropy is a measure of how random or uncertain an intensity pair distribution is. The probability is multiplied by the probability's logarithm, and the result is negated to determine the contribution of entropy. Each intensity pair's entropy contribution (E_C) is tallied up and added to the total entropy value in Equation (20). The distribution of intensity pairs

across the entire image is represented by the average amount of information or randomness by the overall entropy.

g. Return the calculated entropy value

h. Similarly, other significant features Energy, Contrast, Correlation and Homogeneity are computed and they are provided by

$$\text{Energy} = \sum\left(\text{GLCM}_{\text{normalized}}(i,j)\right)^2 \text{.....(21)}$$

The energy feature is calculated in equation (21) by adding the squared probabilities of all intensity pairs. The uniformity or homogeneity of the image as a whole is reflected in the energy. The distribution of intensity pairs is more uniformly distributed at higher energy values.

$$\text{Contrast} = \sum(i-j)^2 * \text{GLCM}_{\text{normalized}}(i,j) \text{ .....(22)}$$

By adding the squared differences in intensities (i - j) multiplied by the corresponding probability, equation (22) calculates the contrast feature. The local variations or differences between intensity pairs are measured by contrast. The difference between adjacent intensities is greater when the contrast value is higher.

$$\text{Correlation} = \frac{\sum\left((i-\text{Mean}_i)*(j-\text{Mean}_j)*\text{GLCM}_{\text{normalized}(i,j)}\right)}{\text{StdDev}_i * \text{StdDev}_j} \text{ .....(23)}$$

By taking into account the intensities' mean values and standard deviations, equation (23) calculates the correlation feature. It gauges the spatial dependence of intensities and their linear relationship. A stronger linear relationship between intensities is indicated by higher correlation values.

$$\text{Homogeneity} = \sum\left(\frac{\text{GLCM}_{\text{normalized}}(i,j)}{(1+|i-j|)}\right) \text{.....(24)}$$

By adding the normalised probabilities of intensity pair divisions by the absolute difference in intensities (1 + |i - j|), equation (24) calculates the homogeneity feature. The homogeneity of intensity pairs is a measure of how similar or close they are. A more homogeneous texture with comparable intensities is indicated by higher homogeneity values.

C. Algorithm for Stage 3: PSO

Step i. Pro1vide the extracted features from GLCM and Initialize the PSO Algorithm

a. Begin the PSO algorithm with its required amount variable

b. Generate an initial swarm of particles:

i. Each particle represents a candidate solution and consists of feature values

c. Perform the PSO optimization loop:

i. Iterate for a specified number of iterations (max_iter)

ii. For each particle in the swarm, Update the particle's velocity using the following formula:

$v = w * v + c1 * rand() * (P_{Best} - C_p) + c2 * rand() * (G_{Best} - C_p)$….(25)

Where

particle best position $= P_{Best}$, Current Position = $C_{p,}$ global best position $= G_{Best}$, Velocity = v , rand() generates a random number between 0 and 1

The formula given by (25) updates each particle's velocity by combining these elements, enabling it to adjust its movement and explore the search space in search of more effective solutions. In particle swarm optimisation (PSO) algorithms, the velocity update is a crucial step that enables particles to move towards advantageous areas of the solution space.

iii. Update the particle's position:

$position = C_p + v$……………………………………………..(26)

In order to determine the particle's new position, equation (26) merely adds the particle's current velocity to its current position. This revision depicts the particle's motion in the solution space based on its present velocity. The PSO algorithm explores and looks for optimal or nearly optimal solutions in the problem space while updating the positions of each particle in real-time.

iv. Clip the position values to ensure they remain within the specified bounds

v. Evaluate the fitness of the new position and update when required.

d. Obtain the optimized feature values: The global best-known position represents the optimized feature values after the PSO algorithm convergence

e. Return the optimized feature values for further analysis and classification task

Step ii. The optimized set of features are obtained from the PSO algorithm, which maximizes the fitness based on the objective function.

D. Algorithm for Stage 4: Detection and Classification

Step i. Select a pre-trained CNN model with 4 hidden layers that has been optimized for image classification tasks.

Step ii. Train the CNN model by means of weights using backpropagation and gradient descent.

Step iii. Extract the optimized features from the tumour region of the MR scan images using the trained CNN model.

Step iv. Combine the extracted features with the corresponding tumour labels.

Step v. Split the combined dataset into training and testing sets.

Step vi. Train an SVM classifier using the training set and the optimized features.

a. Initialize the SVM classifier with desired hyperparameter

b. Compute the Gram matrix (K) for the training dataset

$K(i, j) = kernel\_function(feature\_vector\_i, feature\_vector\_j)$ ….(27)

To help the SVM classifier learn the decision boundary that best divides various classes in the input space, we compute the Gram matrix as given in equation (27), which summarizes the connections and similarities between training samples [41].

c. Solve the optimization problem to obtain the support vectors (α) and bias term (b):

Minimize: $0.5 * \sum_{(i=1 \text{ to } N)} \sum_{(j=1 \text{ to } N)} \alpha(i)\alpha(j)y(i)y(j)K(i,j) - \sum_{(i=1 \text{ to } N)} \alpha(i)$ ……..(28)

By minimizing a cost function and adhering to certain constraints, equation (28) represents the optimisation problem in SVM that aims to determine the ideal values for the bias term (b) and support vectors (α).

d. Store the support vectors (SV) and corresponding labels (SV_labels) for later use

Step vii. Test the trained SVM classifier on the testing set to obtain tumour localization results.

a. For each feature vector in the testing dataset, Compute the decision function value (f(x)):

$f(x) = \sum(i = 1 \text{ to } SV_{count})\alpha(i)y(i)\text{kernel function}(SV(i), x) + b$ ….(29)

Step viii. Apply the trained SVM classifier to the entire MR scan image to predict the presence or absence of a tumour in each region.

a. Classify the feature vector based on the decision function value:

i. If $f(x) > 0$, then tumour

ii. If $f(x) <= 0$, then non-tumour

Step ix. Identify the regions predicted as tumour regions based on the SVM classifier's output.

Step x. Use the tumour localization results to locate and segment the brain tumour area in the MR scan image

E. Process flow for Stage 4: Performance Evaluation

Step i. Performance evaluation metrics to assess the accuracy and performance of the proposed approach via various parameters.

a. $\text{Accuracy} = \frac{(TP + TN)}{(TP + TN + FP + FN)}$……………………………………(30)

i. Here TP – True Positive (identified Tumours),

ii. TN – True Negative, FP – False Positive,

iii. FN – False Negative (not identified)

Step ii. Specificity is the proportion of true negatives identified correctly by the model. It indicates the model's ability to correctly classify non-tumour or non-cancer cases.

$\text{Specificity} = \frac{TN}{(TN + FP)}$……………………………………………(31)

Step iii. Sensitivity or Recall is the proportion of true positives that were identified by the

model. It indicates the model's ability to correctly classify tumour or cancer cases.

$$\text{Sensitivity} = \frac{\text{TP}}{\text{TP} + \text{FN}} \quad \text{.....(32)}$$

Step iv. Precision measures the proportion of positive predictions that are actually correct.

$$\text{Precision} = \frac{\text{TP}}{(\text{TP} + \text{FP})} \quad \text{.....(33)}$$

Step v. The F1 score is the harmonic mean of Recall and Precision. It provides a single metric that balances both Recall and Precision.

$$\text{F1 Score} = 2 * \frac{(\text{Precision} * \text{Recall})}{(\text{Precision} + \text{Recall})} \quad \text{.....(34)}$$

4. Experimental Investigations

a. Pre-Processing and Segmentation Results

The Kaggle [37] was used to obtain the input MRI image of a brain tumour shown in Fig. 2. We used an 80-20% split for training and testing with 300 samples available. This means we shuffled the dataset at random and assigned 240 images (80% of 300) to training and 60 images (20% of 300) to testing. This graphic serves as the analysis' starting point, displaying the raw data that will be analyzed and altered in later steps.

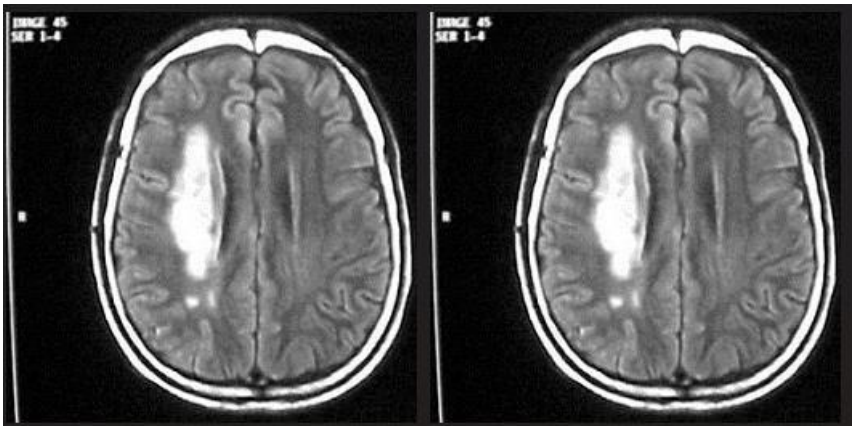

Fig. 2. Input MRI image Fig. 3. Resized Image

Figure 3 shows how to resize an image. An iterative procedure is conducted on each imported image in this step. The purpose is to use bilinear interpolation to resize each image to the desired dimensions. Bilinear interpolation is a technique for estimating pixel values in a scaled image based on the values of nearby pixels. This technique ensures that the image is changed to the necessary size while retaining the original image's overall quality and integrity. Figure 4 shows the pre-processed image after using the Median Filter. The Median Filter is a digital image processing technique for removing noise and artefacts from images. It operates by replacing each pixel value with the median value of the pixels around it. The Median Filter improves the image's clarity and successfully removes undesirable artefacts, resulting in a

cleaner and clearer portrayal of the brain tumour.

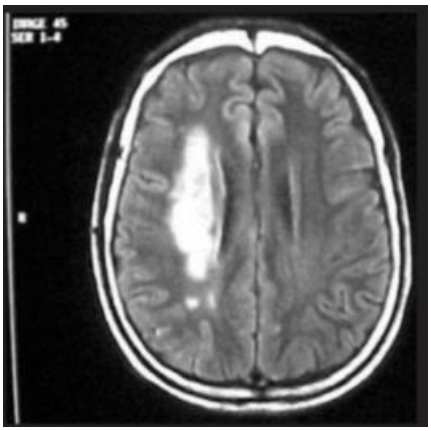

Fig. 4. Pre-processed Image via Median Filter

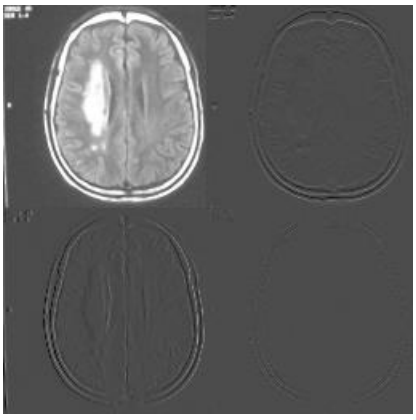

Fig. 5. Haar Wavelet transformation

The Haar Wavelet transformation for decomposition is shown in Figure 5. The Haar Wavelet transformation is a signal and image processing mathematical approach. It decomposes the image into a set of wavelet coefficients that represent the image's various frequency components. At different scales, these coefficients provide useful information on the texture and structure of the image. The Haar Wavelet transformation aids in the extraction of key features and the recording of important details from images, which shall then be used in future analysis phases.

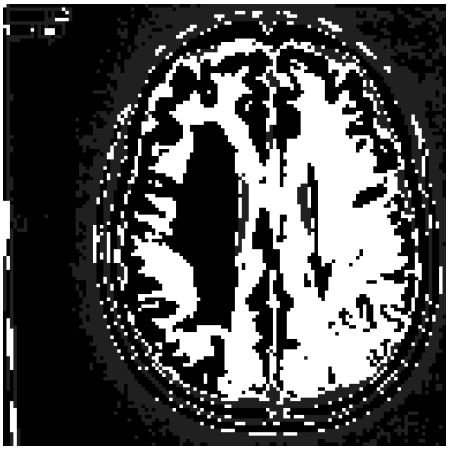

Fig. 6. PSO + CNN segmented image

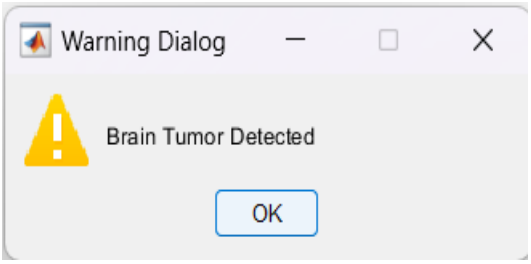

Fig. 7. Dialog box mentioning the stage

The PSO + CNN segmented image is shown in Figure 6. To segment the brain tumour, the optimised features acquired from the Particle Swarm Optimisation (PSO) method are merged with the Convolutional Neural Network (CNN) model in this stage. The PSO method aids in the optimisation of picture characteristics, while the CNN model executes the segmentation process. The segmented image that results emphasises the precise regions related to the tumour, allowing for a clear contrast between the tumour and the surrounding areas.

Figure 7 depicts a dialogue box indicating the state of the process. It is an informative element that indicates the current stage or step in the overall workflow. This dialogue box can display useful information such as the progress of the process, the exact algorithm or technique being used, or any other relevant information to help the user or observer through the process.

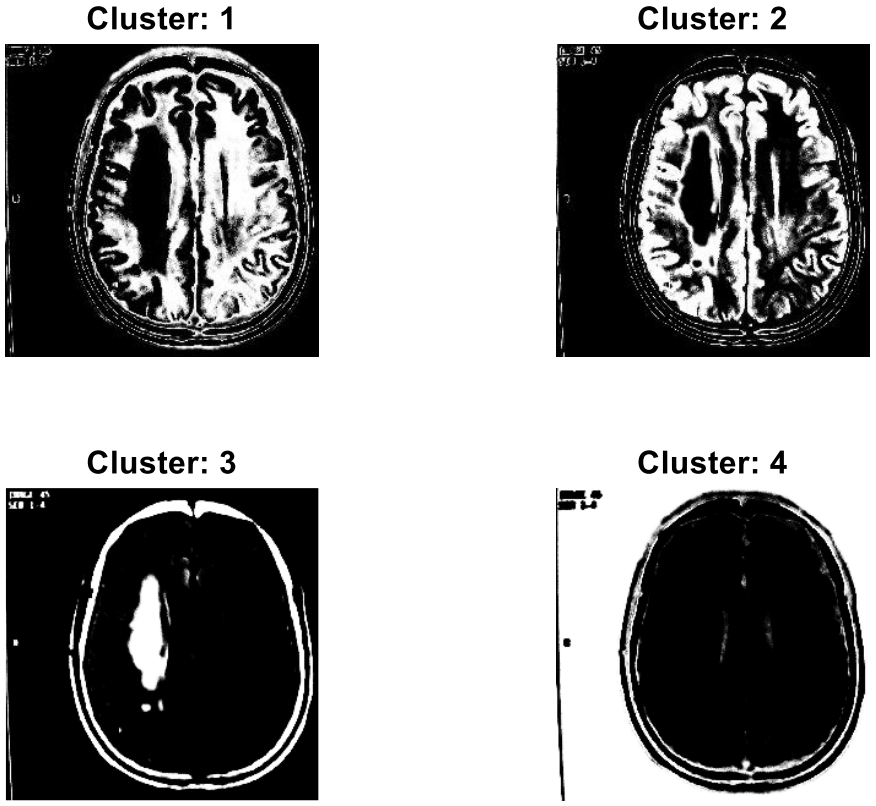

Fig. 8. Image Clusters

Figure 8 depicts the image clusters created by the CNN model's four hidden layers. Hidden layers in the CNN architecture are in charge of extracting and learning complicated characteristics from input images. These layers combine to generate a hierarchical representation of the image, with each layer capturing varying levels of abstraction. The clusters in Fig. 8 show how the CNN model grouped similar features or patterns together, which helps with overall image analysis and interpretation.

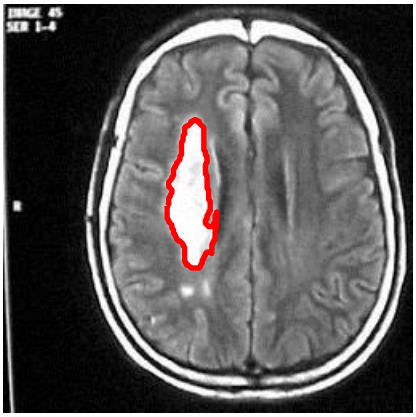

Fig. 9. Tumour Localization Image

Fig. 10. Tumour extracted area

The tumour localization image is shown in Fig. 9. The localization method tries to identify specific regions within the image that contain the tumour once the CNN model and SVM classifier have been trained and tested. This image pinpoints the exact site of the tumour, allowing for more precise examination and diagnosis. Figure 10 depicts the tumour-extracted area. Only the region of interest, which corresponds to the tumour area in the brain scan, is shown in this image. Healthcare practitioners and researchers can focus their attention on the precise region of interest by isolating and extracting the tumour area from the rest of the image, allowing for further analysis, measurement, or additional diagnostic procedures.

b. Feature Extraction

The input MRI image of a brain tumour shown in Fig. 2 was obtained using the Kaggle dataset known as "Brain Tumour MRI Dataset" [37] by Masoud Nickparvar. With 300 samples available, we divided training and testing by 80/20. This means that we randomly shuffled the dataset and assigned 240 images (80% of the total of 300) to training and 60 images (20% of the total of 300) to testing. As the main tool for implementation, MATLAB R2017b was used to carry out the experiment. The testing environment was a PC with an Intel Core i5-8265U CPU operating at a base frequency of 1.60GHz and a maximum turbo frequency of 1.80GHz. The computer had 8.00 GB of installed RAM, of which 7.85 GB were usable. The computer used an x64-based processor and a 64-bit operating system.

For applications in science and engineering, such as image processing, data analysis, and algorithm development, MATLAB R2017b offered a complete environment. The fact that MATLAB was used suggested that the experiment involved numerical computations and probably made use of a variety of built-in functions, toolboxes, and algorithms found within the MATLAB ecosystem.

The PC's hardware configuration, which included an Intel Core i5 processor and 8 GB of RAM, suggested a moderate computing environment suitable for running MATLAB and effectively completing computational tasks. Large datasets and memory-intensive operations were made possible thanks to the 64-bit operating system and x64-based processor's improved system resource utilisation. For the five matched samples that were analysed for the proposed system, the features that were recovered using the feature extraction technique are listed in

Table 2.

Table 2. Features extracted for Samples of Brain Tumour Images

	Sample Brain Tumour Images				
Features Extracted	Sample 1	Sample 2	Sample 3	Sample 4	Sample 5
Entropy	9.8267	9.7467	9.7632	9.7651	9.6529
Contrast	0.525	0.463	0.531	0.5231	0.513
Correlation	0.9246	0.9341	0.9141	0.9136	0.9219
Energy	0.01088	0.01103	0.01058	0.01085	0.01075
Homogeneity	0.4165	0.4173	0.4145	0.4138	0.4147

Table 2 shows the features retrieved from five brain tumour samples in the process. Here GLCM is a texture analysis approach that evaluates the spatial relationships between pixels in an image with different grey levels is utilized to extract features.

Several GLCM properties are determined for each sample, including entropy, contrast, homogeneity, correlation, and energy. These features provide quantitative metrics that define the textural aspects of tumour images, which can help distinguish between different types of tumours or identify anomalies.

The entropy characteristics of the samples are depicted in Fig. 11. Entropy is a measure of the unpredictability or uncertainty in an image's distribution of pixel intensities. High entropy values in brain tumour photos imply a more complicated texture pattern, whilst low entropy values indicate a more uniform or homogenous texture.

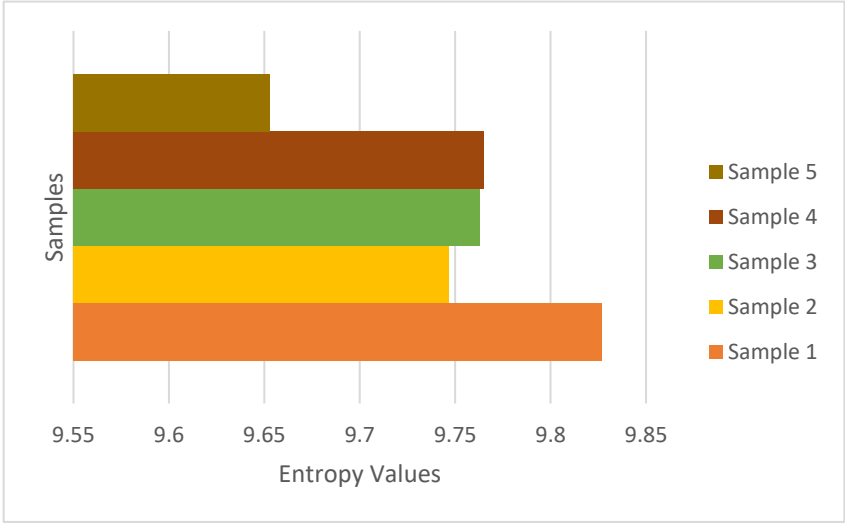

Fig. 11. Entropy Features of Samples

The contrast and homogeneity characteristics of the samples are also shown in Fig. 12. Contrast is the difference in intensity between neighbouring pixels in an image, suggesting the presence of sharp transitions or borders. In contrast, homogeneity assesses the similarity or uniformity of pixel intensities within an image. High contrast values indicate greater intensity differences, whilst high homogeneity values indicate a more uniform texture pattern.

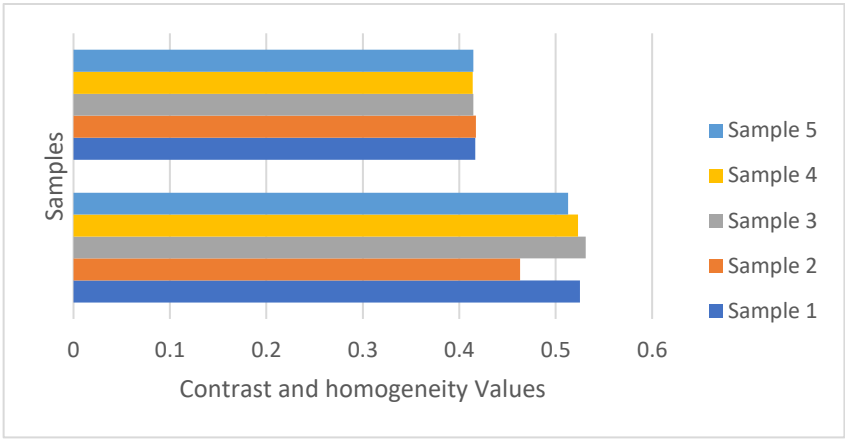

Fig. 12. Contrast and Homogeneity Features of Samples

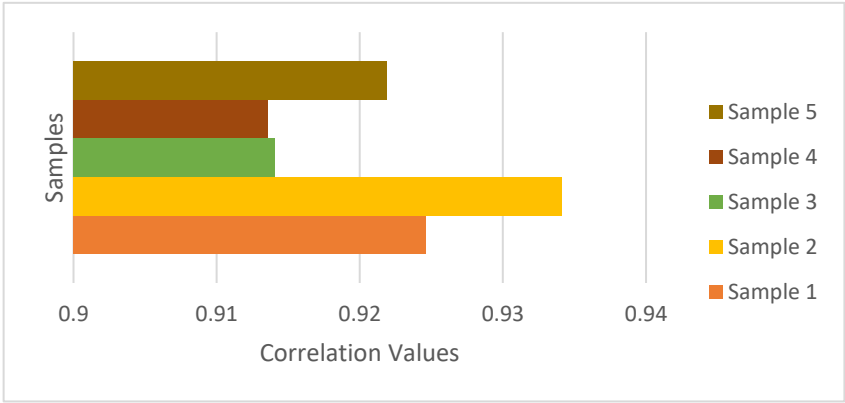

Fig. 13. Correlation Features of Samples

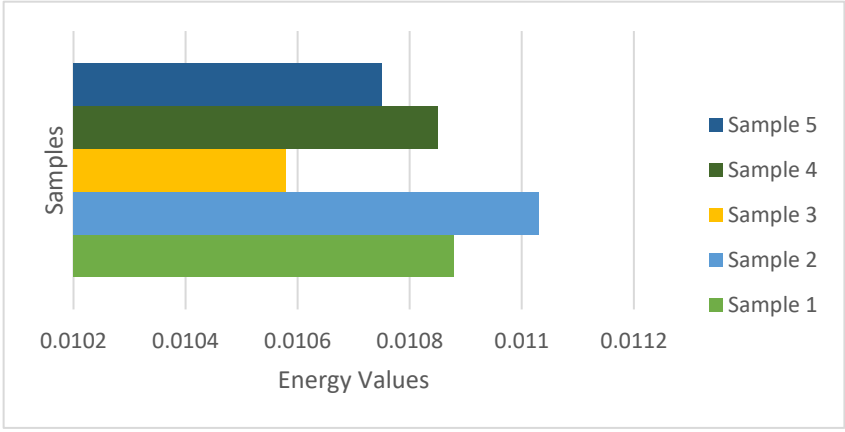

Fig. 14. Energy Features of Samples

The correlation features of the samples are depicted in Fig. 13. Correlation quantifies the linear relationship between pixel intensities in an image. A high correlation value shows a strong

linear link between pixel intensities, whereas a low correlation value indicates a weaker or more scattered association.

Figure 14 depicts the energy characteristics of the samples. Energy is calculated as the sum of squared GLCM values and represents the overall magnitude or strength of the texture pattern in the image. Low energy values indicate a smoother or less pronounced texture, whereas high energy values indicate a more noticeable or dominant texture pattern.

c. Performance Evaluation

Table 3 shows the accuracy values of the proposed methods as well as previous methods such as the RCNN approach [28], the concept of transfer learning [29], a 16-layer VGG-16 deep NN [30], a transfer learning-based Convolutional Neural Network (CNN) [31], PCA+RELM [33], CNN+adam Optimizer [34], Conventional CNN [35], and Deep Learning [36]. The proposed method for diagnosing and localising brain tumours achieved a remarkable 99.8681% accuracy, outperforming previous methods.

Table 3. Accuracy Performance evaluation

Year	Techniques used	Accuracy (%)
2022	RCNN approach [28]	98.21
2021	concept of transfer learning [29]	99.02
2021	a 16-layer VGG-16 deep NN [30]	98
2020	transfer learning-based Convolutional Neural Network (CNN) [31]	94.70
2019	CNN technique + GoogleNet [32]	98
2019	PCA+RELM [33]	94.23
2018	CNN+adam Optimizer [34]	98.51
2018	Conventional CNN [35]	93.68
2017	Deep Learning [36]	91.43
Proposed Method		99.8681

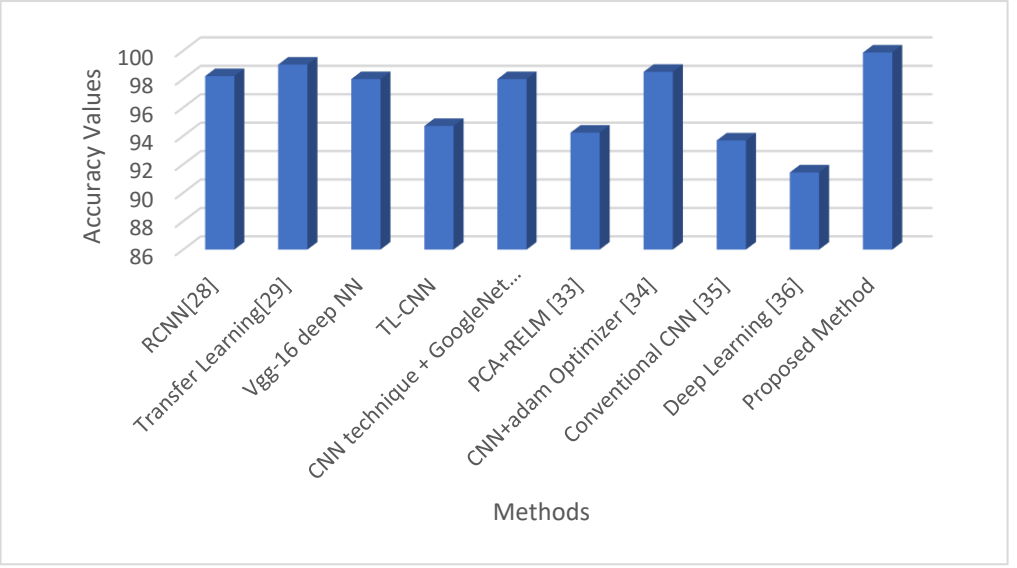

Fig. 15. Accuracy Comparative Plot

Figure 15 shows Comparable Accuracy A comparison of accuracy values (in percentages) on the Y-axis and comparison methods, including the proposed method, on the X-axis is depicted in the plot. The plot shows that the proposed method outperforms the others in terms of accuracy, emphasising its superiority in diagnosing and localising brain tumours.

Table 4 compares the three approaches' sensitivity, accuracy, and F1 score. The classifier's sensitivity denotes its ability to correctly identify positive instances (tumours) that provides an overall assessment of the classifier's performance. The suggested technique has high recall and precision scores, suggesting its accuracy in recognising tumours. The transfer learning-based Convolutional Neural Network (CNN) technique [31] achieves a higher F1 score, indicating a better balance of precision and recall.

Table 4. Sensitivity, Precision and F1 Score Comparison

Year	Techniques used	Sensitivity/Recall (%)	Precision (%)	F1 Score (%)
2020	transfer learning-based Convolutional Neural Network (CNN) [31]	98.70	98.6	99.98
2019	CNN technique + GoogleNet [32]	97.9	99.2	97
2018	Conventional CNN [35]	97.5	91	94.1
2017	Deep Learning [36]	98	93	95
Proposed Method		99.35	99.439	99.225

Figure 16 shows a comparison of sensitivity, accuracy, and F1 score values for various approaches. This plot clearly depicts the performance disparities and underlines the suggested method's capabilities in terms of sensitivity and precision

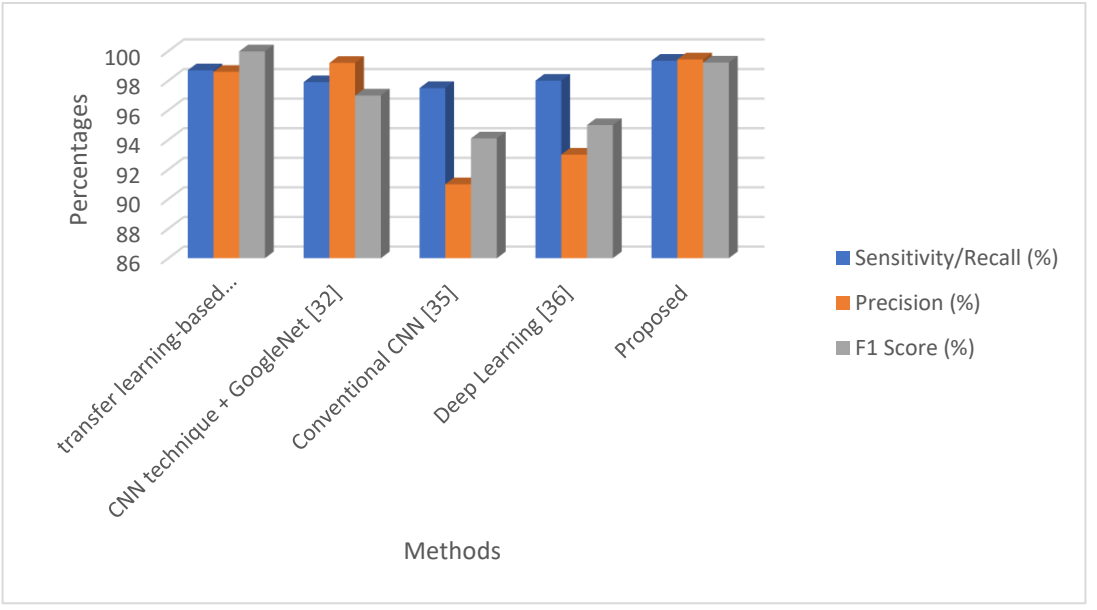

Fig. 16. Sensitivity, Precision and F1 Score Comparison

Table 5 contrasts the specificity parameter, which measures the classifier's ability to properly identify non-tumour negative cases out of all actual negative cases. The proposed method had

a higher specificity value of 99.573% than the CNN methodology + GoogleNet [32], which had a specificity value of 99.4%. This demonstrates the suggested method's robustness and accuracy in correctly recognising non-tumour zones.

Table 5. Specificity parameter Comparison

Year	Techniques used	Specificity (%)
2023	Chronological Artificial Vultures Optimization (CAVO) [38]	93.8
2022	i-YOLOV5 [39]	98.78
2020	Whale Harris Hawks optimization (WHHO) + deep convolution neural network (DCNN) [40]	79.1
2019	CNN technique + GoogleNet [32]	99.4
Proposed Method		99.573

Figure 17 shows a comparison plot of specificity values to show where the proposed method sits in terms of specificity performance

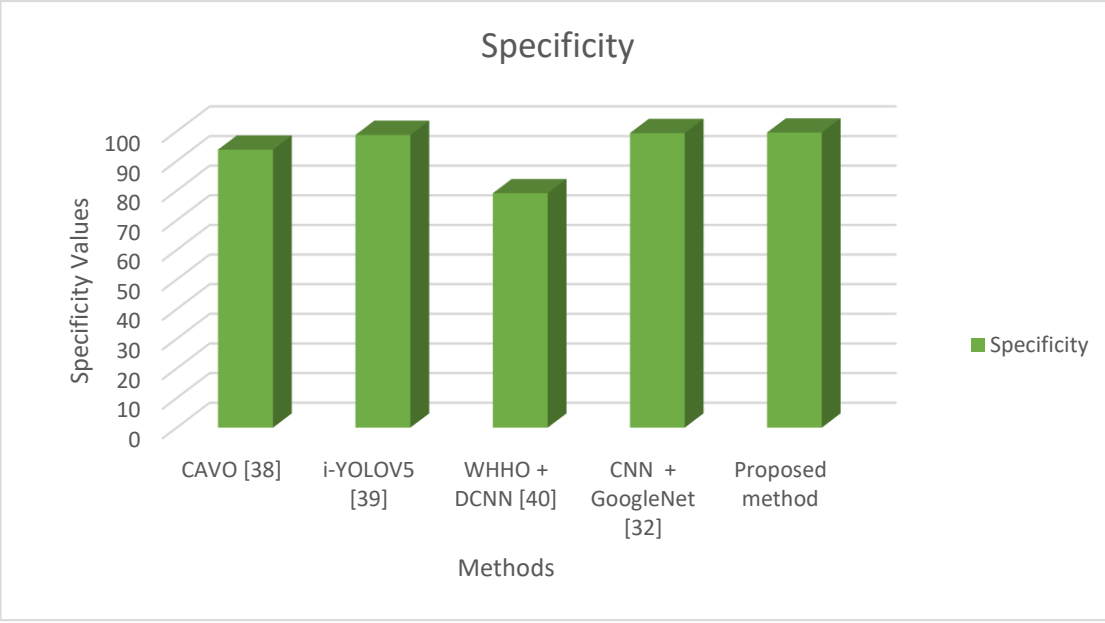

Fig. 17. Specificity values Comparison

Finally, the proposed method in this work exhibits outstanding accuracy, sensitivity, precision, and specificity in the detection and localization of brain tumours. It outperforms various existing methods described in the literature in terms of accuracy, recall, precision, F1 score, and specificity. These findings show the suggested method's effectiveness and potential as a valuable tool for accurate brain tumour analysis and diagnosis, holding tremendous promise in the field of medical imaging and healthcare.

5. Conclusion and Future Scope

Eventually, employing MRI data, this study proposes an integrated hybrid technique for efficient brain tumour analysis. The proposed method is organised into five steps, each of which addresses a distinct component of the analysis process and dataset used is collected from the open source Kaggle database. Scaling and filtering procedures are used in the pre-processing stage to standardise and improve the properties of MRI scans. GLCM approach is used in the feature extraction step to distinguish between tumour and non-tumour regions based on statistical features. Then, Particle Swarm Optimisation (PSO) is used to optimise individual features in order to improve analysis speed. In the fourth stage, a CNN and SVM combination is used for tumour detection and classification, allowing for exact tumour location. In the last stage, the proposed hybrid technique is tested, with excellent metrics such as high specificity (99.573%), accuracy (99.8681%), precision (99.439%), recall (98.45%), and F1 score (99.225%). These findings emphasise the proposed method's accuracy and efficiency in brain tumour analysis. The primary purpose of this study is to address the demand for better brain tumour diagnosis by developing an accurate and efficient analysis approach. To provide a reliable and precise analysis of brain tumours, the integrated hybrid technique integrates preprocessing, feature extraction, optimisation, detection, and classification. The proposed method outperforms existing approaches in the literature due to the incorporation of several strategies and algorithms.

While the proposed hybrid technique has yielded promising results in the investigation of brain tumours, there are various opportunities for future research and enhancements, including Extending the dataset used for training and evaluation can increase the proposed method's performance and generalizability. Access to larger and more diversified information can help the model detect and classify brain tumours more correctly. Integrating Advanced Deep Learning Techniques Later: Investigating the integration of more advanced deep learning techniques, such as recurrent neural networks or attention processes, can potentially improve the accuracy and resilience of the tumour detection and classification process. Including Multimodal Imaging in the Future: Integrating several imaging modalities, such as MRI, CT scans, or PET scans, can provide complementary data and increase overall accuracy of brain tumour analysis. Future research should focus on developing algorithms that can successfully combine information from many modalities. Finally, extending the proposed technology to real-time analysis could be advantageous for clinical applications. The development of fast algorithms and hardware implementations capable of processing MRI data in real-time can considerably increase the system's performance and usefulness.

Overall, the proposed hybrid technique lays the groundwork for future advances in brain tumour analysis. This strategy has the potential to improve brain tumour detection and therapy by resolving constraints and embracing future research paths, ultimately leading to better patient outcomes.

References

1. Al-Galal, S.A.Y.; Alshaikhli, I.F.T.; Abdulrazzaq, M.M. MRI brain tumour medical images analysis using deep learning techniques: A systematic review. Health Technol. 2021, 11, 267–

282.
2. Rahman, M.L.; Reza, A.W.; Shabuj, S.I. An internet of things-based automatic brain tumour detection system. Indones. J. Electr. Eng. Comput. Sci. 2022, 25, 214–222
3. 8. Gordillo N., Montseny E., Sobrevilla P. State of the art survey on MRI brain tumour segmentation. Magn. Reson. Imaging. 2013;31:1426–1438. doi: 10.1016/j.mri.2013.05.002.
4. 9. Jayadevappa D., Kumar S.S., Murty D.S. Medical image segmentation algorithms using deformable models: A review. IETE Tech. Rev. 2011;28:248–255. doi: 10.4103/0256-4602.81244.
5. 10. Yazdani S., Yusof R., Karimian A., Pashna M., Hematian A. Image segmentation methods and applications in MRI brain images. IETE Tech. Rev. 2015;32:413–427. doi: 10.1080/02564602.2015.1027307.
6. Zhao, X.; Wu, Y.; Song, G.; Li, Z.; Zhang, Y.; Fan, Y. A deep learning model integrating FCNNs and CRFs for brain tumour segmentation. Med. Image Anal. 2018, 43, 98–111.
7. Singh, N.; Jindal, A. Ultra sonogram images for thyroid segmentation and texture classification in diagnosis of malignant (cancerous) or benign (non-cancerous) nodules. Int. J. Eng. Innov. Technol. 2012, 1, 202–206.
8. Christ, M.C.J.; Sivagowri, S.; Babu, P.G. Segmentation of brain tumours using Meta heuristic algorithms. Open J. Commun. Soft. 2014, 1, 1–10.
9. Singh, L.; Chetty, G.; Sharma, D. A novel machine learning approach for detecting the brain abnormalities from MRI structural images. In IAPR International Conference on Pattern Recognition in Bioinformatics; Springer: Berlin, Germany, 2012; pp. 94–105.
10. Akil M, Saouli R, Kachouri R et al (2020) Fully automatic brain tumour segmentation with deep learning-based selective attention using overlapping patches and multi-class weighted cross-entropy. Med Image Anal 63:101692
11. Akkus Z, Galimzianova A, Hoogi A, Rubin DL, Erickson BJ (2017) Deep learning for brain MRI segmentation: state of the art and future directions. J Digit Imag 30(4):449–459
12. Bernal J, Kushibar K, Asfaw DS, Valverde S, Oliver A, Martí R, Lladó X (2018) Deep convolutional neural networks for brain image analysis on magnetic resonance imaging: a review. Artificial intelligence in medicine
13. A. Auvinen, Y.M. Hakama, Cancer screening: theory and applications. International Encyclopedia of Public Health, Elsevier, 2017, pp. 389–405, https://doi.org/ 10.1016/B978-0-12-803678-5.00050-3.
14. R. Huang, J. Boltze, Y.S. Li, Strategies for improved intra-arterial treatments targeting brain tumours: a systematic review, Front. Oncol. 10 (2020), https://doi. org/10.3389/fonc.2020.01443.
15. Bernal J, Kushibar K, Asfaw DS, Valverde S, Oliver A, Martí R, Lladó X (2019) Deep convolutional neural networks for brain image analysis on magnetic resonance imaging: a review. Artif Intell Med 95:64–81
16. K. Doi, Computer-aided diagnosis in medical imaging: historical review, current status and future potential, Computerized medical imaging and graphics 31 (4-5) (2007) 198–211.
17. T.M. Mack, What a cancer is. Cancers in the Urban Environment, Elsevier, 2021, pp. 5–8, https://doi.org/10.1016/B978-0-12-811745-3.00003-3.
18. M. Lavin, M. Nathan, System and method for managing patient medical records, uS Patent 5,772,585 (Jun. 30 1998).
19. R. H. Taylor, A. Menciassi, G. Fichtinger, P. Fiorini, P. Dario, Medical robotics and computer-integrated surgery, in: Springer handbook of robotics, Springer, 2016, pp. 1657– 1684.
20. Pagadala, P.K., Pinapatruni, S.L., Kumar, C.R., Katakam, S., Peri, L.S.K., Reddy, D.A. (2023). Enhancing lung cancer detection from lung CT scan using image processing and deep neural networks. Revue d'Intelligence Artificielle, Vol. 37, No. 6, pp. 1597-1605. https://doi.org/10.18280/ria.370624

21. G. Litjens, T. Kooi, B. E. Bejnordi, A. A. A. Setio, F. Ciompi, M. Ghafoorian, J. A. van der Laak, B. Van Ginneken, C. I. S´anchez, A survey on deep learning in medical image analysis, Medical image analysis 42 (2017) 60–88.
22. D. N. Louis, A. Perry, G. Reifenberger, A. Von Deimling, D. Figarella-Branger, W. K. Cavenee, H. Ohgaki, O. D. Wiestler, P. Kleihues, D. W. Ellison, The 2016 world health organization classification of tumours of the central nervous system: a summary, Acta neuropathologica 131 (6) (2016) 803– 820.
23. Bengio, Y., Courville, A. C., & Vincent, P. (2012). Unsupervised feature learning and deep learning: A review and new perspectives. CoRR, abs/1206.5538, 1, 2012.
24. Cetin, O., Seymen, V., & Sakoglu, U. (2020). Multiple sclerosis lesion detection in multimodal MRI using simple clustering-based segmentation and classification. Informatics in Medicine Unlocked, 20, 100409.
25. Raja, P. S. (2020). Brain tumour classification using a hybrid deep autoencoder with Bayesian fuzzy clustering-based segmentation approach. Biocybernetics and Biomedical Engineering, 40(1), 440-453.
26. L. A. J. Prabhu and A. Jayachandran, "Mixture model segmentation system for parasagittal meningioma brain tumour classification based on hybrid feature vector," Journal of Medical Systems, vol. 42, no. 12, pp. 1–6, 2018.
27. N. Sengupta, C. B. McNabb, N. Kasabov, and B. R. Russell, "Integrating space, time, and orientation in spiking neural networks: a case study on multimodal brain data modeling," IEEE Transactions on Neural Networks and Learning Systems, vol. 29, no. 11, pp. 5249–5263, 2018.
28. M. Billah, S. Waheed, and M. M. Rahman, "An automatic gastrointestinal polyp detection system in video endoscopy using fusion of color wavelet and convolutional neural network features," International Journal of Biomedical Imaging, vol. 2017, Article ID 9545920, 2017.
29. Kesav, N.; Jibukumar, M. Efficient and low complex architecture for detection and classification of Brain Tumour using RCNN with Two Channel CNN. J. King Saud Univ.-Comput. Inf. Sci. 2022, 34, 6229–6242
30. . Özlem, P.; Güngen, C. Classification of brain tumours from MR images using deep transfer learning. J. Supercomput. 2021, 77, 7236–7252
31. Srikanth, B.; Suryanarayana, S.V. Multi-Class classification of brain tumour images using data augmentation with deep neural network. Mater. Today Proc. 2021.
32. Tandel, G.S.; Balestrieri, A.; Jujaray, T.; Khanna, N.N.; Saba, L.; Suri, J.S. Multiclass magnetic resonance imaging brain tumour classification using artificial intelligence paradigm. Comput. Biol. Med. 2020, 122, 103804. . 103804.
33. Deepak, S.; Ameer, P. Brain tumour classification using deep CNN features via transfer learning. Comput. Biol. Med. 2019, 111, 103345.
34. Gumaei A, Hassan MM, Hassan MR, Alelaiwi A, Fortino G. A Hybrid feature extraction method with regularized extreme learning machine for brain tumour classification. IEEE Access. 2019;7:36266–73
35. Abiwinanda N, Hanif M, Hesaputra ST, Handayani A, Mengko TR. Brain tumour classification using convolutional neural network. In: World congress on medical physics and biomedical engineering 2018. Singapore: Springer; 2019. p. 183–9.
36. Pashaei A, Sajedi H, Jazayeri N. Brain tumour classification via convolutional neural network and extreme learning machines. In: 2018 8th international conference on computer and knowledge engineering (ICCKE). IEEE; 2018 Oct 25. p. 314–9.
37. Paul JS, Plassard AJ, Landman BA, Fabbri D. Deep learning for brain tumour classification. In: Paper presented at the Medical Imaging 2017: Biomedical Applications in Molecular, Structural, and Functional Imaging. 2017.
38. Msoud Nickparvar. (2021). Brain Tumour MRI Dataset. Kaggle. https://doi.org/10.34740/KAGGLE/DSV/2645886

39. Geetha M, Prasanna Lakshmi K, Sajeev Ram Arumugam & Sandhya N (2023) Conditional random field-recurrent neural network segmentation with optimized deep learning for brain tumour classification using magnetic resonance imaging, The Imaging Science Journal, DOI: 10.1080/13682199.2023.2178611
40. Sivapathi Arunachalam & Gopalakrishnan Sethumathavan (2022) An effective tumour detection in MR brain images based on deep CNN approach: i-YOLOV5, Applied Artificial Intelligence, 36:1, DOI: 10.1080/08839514.2022.2151180
41. Rammurthy D, Mahesh PK (2020) Whale Harris Hawks optimization based deep learning classifier for brain tumour detection using MRI images. J King Saud Univ Comput Inf Sci 1–14.